Hydrogen in α-iron: Stress and diffusion

J. Sanchez,[1] J. Fullea,[1] C. Andrade,[1] and P. L. de Andres[2]

[1]*Instituto de Ciencias de la Construccion Eduardo Torroja, CSIC, C/Serrano Galvache 4, E-28033 Madrid, Spain*

[2]*Instituto de Ciencia de Materiales de Madrid, CSIC, Cantoblanco, E-28049 Madrid, Spain*

First-principles density-functional theory has been used to investigate equilibrium geometries, total energies, and diffusion barriers for H as an interstitial impurity absorbed in α-Fe. Internal strains/stresses upon hydrogen absorption are a crucial factor to understand preferred absorption sites and diffusion. For high concentrations, H absorbs near the octahedral site favoring a large tetragonal distortion of the bcc lattice. For low concentration, H absorbs near the tetrahedral site minimizing the elastic energy stored on nearby cells. Diffusion paths depend on the concentration regime too; hydrogen diffuses about ten times faster in the distorted body-centered-tetragonal (bct) lattice. External stresses of several GPa modify barriers by $\approx 10\%$, and diffusion rates by $\approx 30\%$.

PACS number(s): 66.30.J−, 68.43.Bc, 71.15.Mb

I. INTRODUCTION AND METHODOLOGY

Hydrogen embrittlement is believed to be one of the main reasons for cracking of steel structures under stress.[1–3] High strength steels often include a ferritic core made of α-iron (body-centered-cubic lattice, bcc). To control and prevent the cracking of steel it is necessary to understand the chemical and physical properties of hydrogen inside bcc iron. In particular, it has been argued in the literature that the size of the interstitial H [e.g., ≈ 0.3–0.4 Å (Ref. 4)] is too large to fit and diffuse easily in the iron bcc lattice.[5] This argument has also been used to favor absorption on the T-site because it is larger than the O-site.[6] Arguments based on "apparent" sizes of atoms and a static lattice yield a useful basic approximation but leave out important factors. Only a truly microscopic understanding of hydrogen dissolved in iron, including diffusion processes and fully accounting for forces and stresses inside the host matrix, could lead to answers to the many questions arising from experiments. Internal stresses are therefore key to understand the preferred absorption site. Furthermore, external stresses can be used to modify diffusion barriers because they can help to stabilize/destabilize strains originating inside the material to accommodate the absorbed impurity. Owing to its interest, hydrogen absorbed in iron has been studied using different approaches, both from a theoretical and experimental point of view. Unfortunately, a clear consensus about fundamental questions, like the nature of the equilibrium absorption site, the reasons for H to prefer some regions over others, or how to modify the diffusion barriers has not been reached yet. Many theoretical papers have favored hydrogen absorbed in the tetrahedral site (T-site),[7–12] some have preferred the octahedral one (O-site),[13] and others have reported that they are almost equivalent[14] (Fig. 1). From an experimental point of view, it has been generally believed that hydrogen has low solubility and high mobility in bcc iron. However, some recent experiments have attained high concentrations,[15,16] at least locally. Furthermore, experimental evidence has been reported showing that hydrogen might at least partly be found on the O-site.[15] Finally, diffusion barriers that change with the amount of H admitted into the material have been reported in

the literature.[17] In our calculations, we find that both sites are indeed quite similar in energies, the delicate energetic balance between them depending on the stress distribution created by the interstitials. In turn, this depends on the hydrogen concentration, which can be related to locally inhomogeneous regions or more generally to its homogeneous averaged value.

Our methodological approach simulates the atomic absorption and diffusion of hydrogen in the body-centered-cubic iron lattice from first principles. Absorption in high-symmetry sites for different hydrogen loads (densities) has been explored and the internal strains/stresses have been calculated. Diffusion barriers between these stationary absorption sites have been obtained, and the effect of external stresses on diffusion coefficients has been analyzed. Our *ab initio* calculations are based on the density functional theory (DFT) formalism[18] and the theory of pseudopotentials.[19] A periodic supercell is considered to minimize absorbate-absorbate interactions [periodicity is $n \times n \times n$ with respect to a single cubic bcc unit cell (UC)]. One H atom has been located in this supercell, determining the ratio H:Fe from $\frac{1}{2}$ for the $1 \times 1 \times 1$ to $\frac{1}{54}$ for the $3 \times 3 \times 3$. Within this theoretical framework the accuracy of calculations mainly depend on the quality of the pseudopotential, the energy cutoff (E_{ctf}), and the density of the k-point mesh in the irreducible part of the Brillouin zone (BZ) [a Monkhorst-Pack (MP) set of special k-points[20]]. Calculations are performed with CASTEP,[21,22] where a plane-wave basis is used to expand electronic states (spin-polarized bands are considered to account for magnetism in iron). An ultrasoft pseudopotential ($3d^6 4s^2$) including
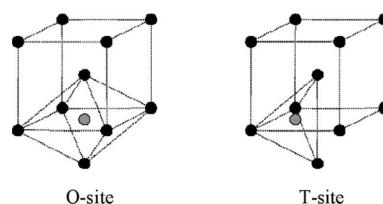

FIG. 1. High-symmetry sites for H absorption inside α-iron: The octahedral (O-site) and tetrahedral (T-site) sites (gray) are shown along with iron atoms in the bcc lattice (black).

a nonlinear core correction is used to describe iron atoms. The exchange and correlation contribution to the total energy is computed within a generalized gradient approximation given by Perdew, Burke and Ernzerhof.[23] An all-bands variational method is used to achieve self-consistency[24] (to improve convergence a smearing width of 0.1 eV has been used). Minimum thresholds to consider the calculations converged after optimization of the geometry are as follows: variations in the total energy $\leq 10^{-5}$ eV, maximum residual force on any atom ≤ 0.01 eV, maximum residual stress on the UC ≤ 0.02 GPa, maximum change in any atom position ≤ 0.001 Å, and maximum change in any cell vector ≤ 0.01 Å. These thresholds are enough for our purposes, but on some particular cases lower thresholds were considered when higher precision was desirable.

II. REFERENCE CALCULATIONS FOR α-IRON AND H

The adequacy of the theoretical framework and the different convergence thresholds has been tested by computing a number of known properties for clean α-iron and atomic and molecular hydrogen separately. For iron, a global energy minimum is found for a bcc lattice (hereafter referred to as the $1 \times 1 \times 1$) with $a=b=c=2.815$ Å ($\alpha=\beta=\gamma=90°$), a predicted magnetization of $2.25\mu_B$, a bulk modulus of 175 GPa, and a Poisson ratio of 0.30. Residual forces on the atoms in the bcc unit cell are $\leq 4 \times 10^{-6}$ eV/Å, residual stress is $\leq 9 \times 10^{-4}$ GPa, and the total energy has been converged to $\leq 10^{-6}$ eV. The computed magnitudes are to be compared with the experimental values 2.867 Å, $2.22\mu_B$, 170 GPa, and 0.29.[25] Fractional errors are 1.8%, 1.4%, 3%, and 4%, respectively, showing the accuracy of this kind of theoretical modeling to describe relevant properties of bcc iron. It is interesting, however, to notice that these quantities show oscillatory convergence as a function of the energy cutoff (E_{ctf}) and the number of k-points; convergence of physical properties has to be established carefully to make sure the oscillations are damped enough as to avoid agreements that might not be stable (Fig. 2). Properly converged values were obtained with $E_{ctf}=375$ eV and a $25 \times 25 \times 25$ MP mesh (455 points in the irreducible part of the Brillouin zone). However, values derived with $E_{ctf}=375$ eV and a $14 \times 14 \times 14$ mesh can be considered enough accurate for our purposes and most of our calculations below for the $1 \times 1 \times 1$ bcc unit cell have been performed with these parameters. Calculations in $n \times n \times n$ unit cells ($n=2,3$) have been performed with $4 \times 4 \times 4$ and $1 \times 1 \times 1$ MP meshes, respectively. These theoretical calculations yield a detailed microscopic picture for the chemistry and the physics governing the material: Iron atoms form metallic bonds of length 2.44 Å, favoring a ferromagnetic alignment of spins mostly residing in the regions around the atoms. Bonding is such that the atomic s level of iron is depopulated in favor of d and p-levels (a Mulliken analysis shows that $\approx 1.3\ e$ is transferred). Although this work is not concerned with face-centered-cubic iron (γ-iron), we notice that this formalism predicts that the next stable phase of iron (fcc) is about 0.1 eV/atom higher in energy, with $a=b=c=3.479$ Å (experimental value is 3.647 Å, a 5% discrepancy), and a magnetization lower by about a fac-
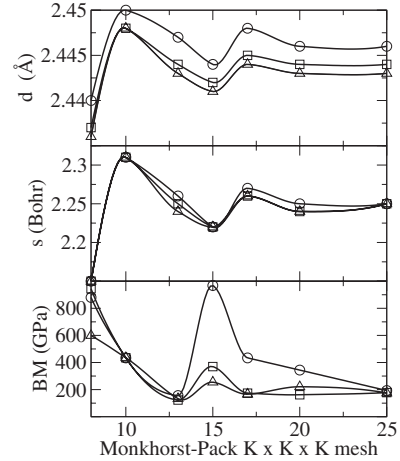

FIG. 2. Convergence of primitive unit-cell parameter (d in Å) (upper panel), magnetization (in units of the Bohr magneton) (middle panel), and bulk modulus (GPa) (lower panel) versus the energy cutoff (circles: 330 eV, squares: 350 eV, triangles: 370 eV), and the $K \times K \times K$ index for the Monkhorst-Pack mesh ($K=25$ results in a mesh of 455 points sampling the Brillouin zone).

tor of 2 due to disorder in the spin orientations. Calculations for H and H_2 have been performed on a $10 \times 10 \times 10$ Å supercell (only the Γ point in the BZ), predicting a bond length and a binding energy for the molecule within 0.5% and 5% from experimental values. The interaction between isolated atoms of H and Fe is moderately weak, with a bonding distance of 1.54 Å and a binding energy of $E_B = E_{FeH} - (E_{Fe} + E_H) = -2.41$ eV (notice that the binding energy is quoted from the electronic energy alone and zero-point vibrations have not been considered). This is corroborated by the very weak interaction of H with Fe_2; the binding energy stays nearly the same (-2.43 eV) in a geometrical configuration where H prefers to interact with only one of the Fe in the dimer. Molecular H_2 has been reported to dissociate on iron surfaces,[12] in addition we do not find a tendency for hydrogen atoms inside iron to reform molecules. As an example, we compare for the $2 \times 2 \times 2$ unit cell ($Fe_{16}H_2$) the total energies of two H atoms located in nearby two different octahedral sites (H-H distance is ≈ 2 Å) and a single H_2 molecule. The dissociated state is favored by $E_{2H} - E_{H_2} = -3.3$ eV (we notice that the energy gain comes partially from the smaller stress that the two separated H atoms introduce in the iron lattice compared with the one originated from the single H_2 molecule). Therefore, we conclude that it is not necessary to study processes related to molecular H_2 inside α-iron.

III. HYDROGEN IN IRON: HIGH CONCENTRATION

Even if the density of hydrogen absorbed in iron is expected to be small on the average, it can accumulate locally on some regions where the density can be high. Indeed, important changes in the elastic properties of iron are found in these regions. Furthermore, experimental evidence of high-density phases have been reported in the literature.[15,16] Therefore, we find it interesting to analyze the stoichiometry

TABLE I. For different concentrations and systems, energy differences between the O-site and T-site sites (ΔE in meV), and fractional changes in the unit-cell volume for O-site and T-site ($\frac{\Delta V}{V_0}$).

Density				
	System	ΔE	$\frac{\Delta V}{V_0}|_O$	$\frac{\Delta V}{V_0}|_T$
Fe$_2$H	Tetragonal	-53	0.12	0.16
	Cubic	452	0.19	0.16
	$1\times1\times1$	612	0.00	0.00
Fe$_{16}$H	Tetragonal	119	0.03	0.03
	Cubic	169	0.03	0.03
	$2\times2\times2$	117	0.00	0.00
Fe$_{54}$H	Tetragonal	105	0.004	0.003
	Cubic	115	0.004	0.004
	$3\times3\times3$	108	0.000	0.000

Fe$_2$H. In the bcc lattice two high-symmetry sites (O-site and T-site) compete to locate the interstitial atom, and diffusion through the iron matrix takes place along paths joining them. We simultaneously optimize all the geometrical parameters to reach a global minimum in the total energy and small residual forces in any atom in the model. The three vectors defining the periodic lattice have been kept orthogonal ($\alpha = \beta = \gamma = 90°$). The lengths of these vectors have been optimized taking into account the following cases: (a) independent optimization (resulting in tetragonal systems), (b) optimization subject to the condition $a=b=c$ (cubic system), and (c) no optimization, merely scaling the clean bcc unit cell (the system is under stress, especially for high concentrations of the interstitial). Starting with model (a) and allowing the lattice to relax completely, we have reached a best configuration with residual forces $\leq 10^{-4}$ eV/Å and residual stresses $\leq 5\times10^{-4}$ GPa (the energy change was $\leq 2 \times 10^{-6}$ eV and the maximum final displacement of any atom was $\leq 5\times10^{-4}$ Å). Under these conditions, the O-site is the global minimum, the T-site being higher in energy by 53 meV (Table I). To reach this configuration, the lattice suffers a large body-centered-tetragonal (bct) distortion, keeping the $P4/MMM$ symmetry group (16 elements), while the optimum geometry for the fully relaxed lattice for H in the T-site increases the symmetry from $C2$ (4 elements) to $P\text{-}4M2$ (8 elements). Our preferred absorption site is different from the one recently obtained by Jiang and Carter for the same density using a similar formalism.[12] There are several possible sources for this discrepancy, e.g., the pseudopotentials, the exchange and correlation functional, or even the fine details of how different codes reach a self-consistent solution and compute forces on the atoms. We believe these are all unlikely sources to explain the different final configuration due to the excellent performance when comparing different physical magnitudes with experimental data or just between different theoretical methods of similar quality. Jiang and Carter predict for Fe$_2$H that the T-site is preferred over the O-one by 10 meV, while we have found the reversed conclusion by 53 meV. The overall 63 meV discrepancy is indeed a small one, but it seems to be above the noise level expected from the convergence tests. The reason for the difference is

most likely related to the final optimum configuration obtained in each calculation (our final configuration is given in Table II). The energy landscape is a complex one, and the algorithm searching for a global minimum could be trapped in nearby local ones. We have made an effort to minimize residual forces and stresses as much as possible. To search for a global minimum we have used the Broyden-Fletcher-Goldfarb-Shanno algorithm that is known to be a robust one and has been successfully applied both in electronic structure calculations and in low-energy electron diffraction optimization of geometries.[26–28] The resulting bct distortion for H in the O-site is indeed quite big and might be hidden in a difficult landscape; we notice that our optimization under the restriction of an isotropic deformation of the unit cell ($a=b=c$) results in the T-site as the preferred one by 452 meV. Finally, we should comment that although the bct distortion seems significant, in particular because it would favor the bcc to fcc transformation, the discussion here is based solely on electronic energies, and other factors might play an important role too. Configurational disorder is expected to favor T-sites. The relative contribution of entropy to the Helmholtz free energy for T-site and O-site can be estimated from the simple consideration that there are four times more configurations for T-sites. Therefore, T-sites are favored on the grounds of entropic arguments by $k_BT \log 4$, approximately 34 meV at room temperature, which tends to make the energetic more similar but still is not enough to make the T-site the global minimum. Furthermore, zero-point energy (ZPE) corrections may affect differently the energy of two absorption sites with different coordination and geometrical parameters. A careful determination of the phonon spectra for this system demands the use of a considerable amount of computing time and is planned for a future paper. Our own initial estimates, based on sketchy models that can be solved quickly, result in the O-site getting further stabilized with respect to the T-site by ≈ 20 meV. A word of caution is in order here since these values may have a large error bar that we have not properly estimated. The model used to deduce these values is as follows: the cut-off energy has been reduced to 300 eV, the k-point mesh to a mere $6\times6\times5$, phonons have been estimated only in the Γ point using a finite displacement method (0.00529 Å) and a $2\times2\times2$ supercell. Therefore, these corrections are only to be taken as rough order of magnitude estimates, but in our calculations ZPE does not switch the preferred absorption site. Frequencies in Γ for the O and T sites are all real, marking the character of global and local minima for these sites.

From a physical point of view, in this high-concentration regime, the main characteristic of the tetragonal distortion necessary to accommodate H in the O-site is that it is both large and anisotropic. First, we notice that only occupation of similarly oriented O-sites over many unit cells would allow this kind of distortion. Second, fractional changes in the UC volume are large, $\frac{\Delta V}{V_0} = 0.12$, and 0.16, for O-site and T-site, respectively; this is the trace of the strain tensor and measures the global stress produced by the interstitial. Therefore, it is necessary to understand the stress distribution created around the distorted cell. Total energies for a model where the UC is allowed to relax keeping the cubic UC ($a=b=c$) show that when H is in O the system gains a fair amount of

TABLE II. Optimum geometrical configurations for Fe_2H near the octahedral and tetrahedral sites. Atomic positions, x, y, z, are given in fractional coordinates ($\alpha=\beta=\gamma=90°$). Total energies (in eV) correspond to the optimum geometry. F_{max} and S_{max} are the maximum residual forces on atoms and stresses on the cell. The charge transfer, $\Delta(q)$, is given in units of the electron charge, and the spin is given in units of μ_B (Mulliken analysis).

Octahedral					
Energy (eV)	Spin	F_{max} (eV/Å)	S_{max} (GPa)		
−1748.150	2.40	3×10^{-6}	4×10^{-4}		
a (Å)	b (Å)	c (Å)	c/a	V (Å^3)	$\Delta V/V$ (%)
2.628	2.628	3.618	1.38	24.99	0.12
Atom	x	y	z	$\Delta(q)$	Spin
H	0.5	0.5	0.0	−0.30	−0.02
Fe_a	0.0	0.0	0.0	0.19	1.11
Fe_b	0.5	0.5	0.5	0.10	1.29
Tetrahedral					
Energy (eV)	Spin	F_{max} (eV/Å)	S_{max} (GPa)		
−1748.097	2.46	1×10^{-4}	5×10^{-4}		
a (Å)	b (Å)	c (Å)	c/a	V (Å^3)	$\Delta V/V$ (%)
2.896	2.984	2.984	0.97	25.78	0.16
Atom	x	y	z	$\Delta(q)$	Spin
H	0.2641	0.5	0.0	−0.34	−0.02
Fe_a	0.0	0.0	0.0	0.17	1.24
Fe_b	0.5283	0.5	0.5	0.17	1.24

energy from the anisotropic deformation (510 meV), while when H is near T-site the gain is smaller (9 meV). Under this cubic restriction, the fractional change of the UC volume are 0.19 and 0.16 for O-site and T-site, respectively; the interstitial fits poorly in O in absence of the tetragonal distortion (internal pressure upon injection of the interstitial H in the clean iron bcc lattice amounts to several tens of GPa). From a chemical point of view, the role of the interstitial atom is to debilitate the Fe-Fe nearest-neighbor (NN) interaction; Fe-Fe bond length increases by 0.15 and 0.08 Å for H in O-site and T-site, respectively. In both sites, hydrogen tends to get negatively charged ($0.3e$), while its spin is delocalized contributing little to the total integrated spin density that only increases by $\approx 0.15\mu_B$ with respect to clean bcc Fe. It is worth to notice that the tetragonal distortion of the UC for H absorbed on the O-site ($\frac{c}{a}=1.38$) is not far away from the distortion predicted for Bain's mechanism to transform from α-iron to γ-iron ($\frac{c}{a}=1.41$).[29]

To compute diffusion barriers we have used a linear synchronous-transit method followed by quadratic refinement.[30] In addition, when a reduced number of parameters could be established as the more relevant ones exhaustive searches in regions of interest have been used to display in more detail the topology around the reaction pathway (Fig. 3). We have computed diffusion barriers between the optimum configurations reached for H at O-site and T-site. For the high-density case, the transition state is located in the line joining O-site and T-site, about halfway, with a barrier of $B=70$ meV (Fig. 4). Thermal diffusion can be estimated by considering a typical vibrational frequency for H in the lattice: $W\approx10^{12}$ Hz. Diffusion is quick; hopping from

O-site to T-site happens $D_T(B)=10^{11}$ times per second at room temperature. Quantum diffusion via tunneling through the barrier is important for such a light atom as H. The tunneling rate can be estimated from a one-dimensional WKB
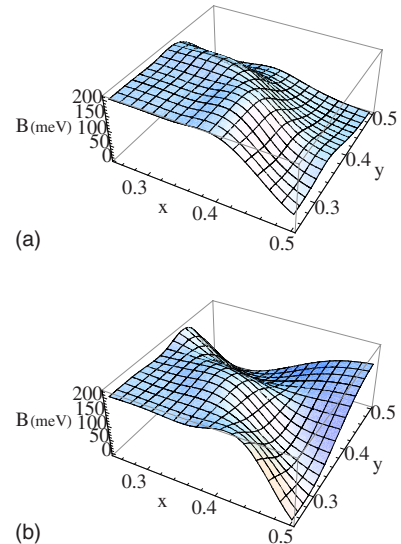

FIG. 3. (Color online) Total energy (meV) landscapes for (a) high- and (b) low-concentration cases (top and bottom panels). x and y are given in fractional units with respect to the $1\times1\times1$ bcc unit cell. O-site is located at the top right corner $\{\frac{1}{2},\frac{1}{2},0\}$, and T-site at the bottom right and top left corners $\{\frac{1}{4},\frac{1}{2},0\}$. The region around the Fe at the origin (higher values than 200 meV) has been artificially put to a constant value to improve visibility of the relevant paths from O-site to T-site (a) and from T-site to T-site (b).
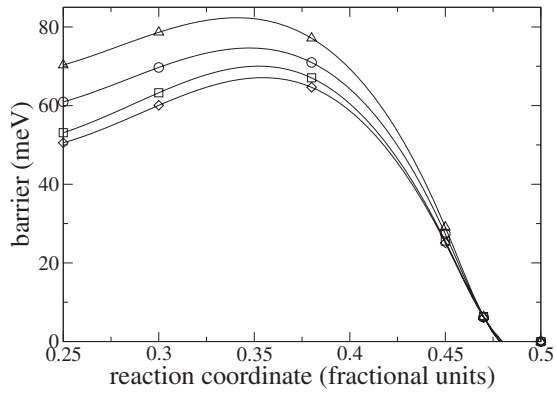
FIG. 4. Diffusion barriers between T-site $\left(\frac{1}{4}\right)$ and O-site $\left(\frac{1}{2}\right)$ along the actual diffusion path (see Fig. 3; the reaction coordinate has been scaled between both end points) for fully relaxed Fe_2H under different external stresses. The triangles (a) and diamonds (d) correspond to hydrostatic pressures of ± 2 GPa (tensile and compressive, respectively), squares (c) to a tensile uniaxial stress of -1 GPa, and circles (b) to 0 GPa. The origin of energies has always been taken as the optimum equilibrium value (for this concentration, the O-site).

approximation, $D_Q(B,d) = We^{-4d\sqrt{2mB}/3}$, where d is the distance between minima (0.6 Å). D_Q is only lower than the thermal one, D_T, by a factor of 6. At low temperature, the tunneling process becomes the main mechanism, being equal in importance to the thermal one at about $T \approx 183$ K, near the liquid-nitrogen temperature. The effect of external stresses on the barrier is shown in Fig. 4. As discussed above, ZPE can affect the energies of different configurations, and in particular it can lower the already small diffusion barriers. The model described above results in a lowering of the barrier as seen from the O-site of ≈ 7 meV, and a lowering of the barrier as seen from the T-site of ≈ 27 meV. We notice that frequencies computed for the threshold shift (TS) now include a single imaginary value, indicating that this is a first-order saddle point. Again, this correction should be taken as a crude estimate and we notice that similar calculations give a correction for the barrier of 46 meV.[12] We estimate that barriers corrected by ZPE should be lower than the ones obtained from total energies only by ≈ 40–50%. A tensile stress of 2 GPa increases or decreases the barrier by about 9%, changing the thermal diffusion by about 30% at room temperature, while the quantum mechanism is affected by 25%. Barriers for this high-concentration scenario have been computed using periodic boundary conditions on a $1 \times 1 \times 1$ unit cell, representing diffusion of H and all the adjacent periodic copies simultaneously (notice that periodic boundary conditions respect the Fe_2H stoichiometry at all times during the diffusion process). Finally, we check the internal consistency of these high-density simulations by considering a $2 \times 2 \times 2$ unit cell, with the same Fe_2H stoichiometry. In this unit cell there are 36 O-sites and 144 T-sites that can be occupied by the 8 H. This makes 10^7 possibilities for octahedral occupation, 10^{12} for tetrahedral occupation, and 10^{13} for an arbitrary mixture of both. A proper study of this system should try to sample these configurations, which is beyond the scope of this work. However, a check for the

consistency of our previous results only needs to consider a few of these configurations. To ascertain the stability of the energy ordering between O and T-sites we consider two configurations where the octahedral/tetrahedral sites are occupied accordingly with results obtained in the $1 \times 1 \times 1$ unit cell (including the respective tetragonal distortions). The length of the vectors and all the atoms in the $2 \times 2 \times 2$ unit cell are allowed to relax in x, y and z directions including 72 degrees of freedom (the center of mass is constrained). A stationary point is considered converged when forces and stresses are below 0.002 eV/Å and 0.005 GPa, respectively. The O-site converges to a better minimum than the T-site by 0.470 eV, which is consistent with the value derived from the $1 \times 1 \times 1$ simulation (0.06×8) with an accuracy of 1.2 meV/$(1 \times 1 \times 1$ unit cell$)$. In this model, if we try to compute the barrier for a single H hopping from the global minimum in the O-site to the T-site, we find that the effect of the occupation of the other seven sites in octahedral positions is to transform this single T-site into a high-order saddle point. H in this T-site relaxes spontaneously to the neighboring O-site. Barriers computed with the help of the $1 \times 1 \times 1$ periodic model correspond to transforming large regions of all O-occupancy into large regions of all T-occupancy. We have not investigated diffusion paths for H in the presence of a given mixture of O-sites and T-sites due to its combinatorial complexity. However, this example shows the interest to further study $n \times n \times n$ cells in the high-density regime in the future, and highlights the impact of the distortion of the lattice on the absorption energy on single local sites.

IV. HYDROGEN IN IRON: LOW CONCENTRATION AND FINITE ELEMENT SIMULATION

We simulate the lower density scenario by placing one H in the $2 \times 2 \times 2$ and $3 \times 3 \times 3$ unit cells ($Fe_{16}H$ and $Fe_{54}H$). At these concentrations, hydrogen is free to move around the lattice without interacting with other hydrogen atoms (the remaining H-H interaction on the $1 \times 1 \times 1$, ≈ 0.06 eV, now becomes negligible). Other convergence parameters are kept the same, except for the k-point mesh, which has been reduced accordingly to the bigger size of the supercell. Now, the global total-energy minimum still happens for a bct lattice, but it moves from the O-site to the T-site, which becomes lower in energy with respect to O by 119 and 105 meV for $Fe_{16}H$ and $Fe_{54}H$, respectively. The change in the unit-cell volume and the tetragonal distortion of the lattice gets smaller with decreasing density, and nearly independent of the absorption site, $\frac{\Delta V}{V_0} = 0.03$ and 0.004, and $\frac{c}{a} = 1.04$ and 1.003, respectively (Table I). The same calculation for a relaxed bcc lattice ($a = b = c = 2.843$ Å) yields a difference of 169 meV in favor of the T-site. Diffusion happens now from T-site to T-site with a barrier of 82 meV (bct) or 127 meV (bcc) [Fig. 3(b)]. This barrier implies a diffusion rate ≈ 10 times slower than for the high-density case. Tunneling is even more reduced, because the distance between minima is larger (≈ 0.9 Å). In T-site, H moderately interacts with four NN at 1.65 Å, and gets negatively charged by $0.33e$. In O, H interacts mainly with two NN, at 1.57 Å, while the next nearest neighbors (NNN) remain at 1.98 Å (H gets a
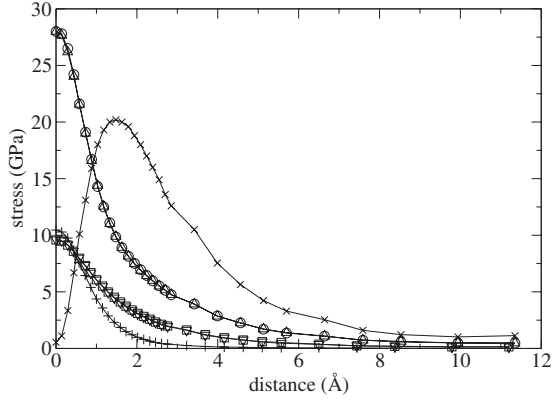
FIG. 5. Finite element simulation of stresses around the fully relaxed $1 \times 1 \times 1$ unit cell upon absorption of H on the O-site (circles, $\bigcirc$, and up-triangles, $\triangle$, in the x and y direction; times, $\times$, in the z one), and T-site (squares, $\square$, and down-triangles, $\triangledown$, in the x and y direction; plus, $+$, in the z one).

similar amount of charge, $0.32e$). Typical displacements for NN with respect to their positions in the clean iron lattice are ≈ 0.1 Å (NN), while NNN and more distant atoms move less than ≈ 0.02 Å. The spin on the different atoms does not show changes which are worthy of comment.

Strains to accommodate the interstitial H create a stress distribution that has been analyzed by a finite element (FE) technique (input parameters have been obtained from our calculations above). Assuming that deformations are elastic, we have computed the stress distribution in the iron matrix and the free-energy variation when H is absorbed in the O-site and T-site. Starting from strains obtained by DFT on the $1 \times 1 \times 1$ supercell, the FE simulation allows us to study its effect in a surrounding region of size $n \times n \times n$ around the original volume ($n=2,5$). Strictly speaking, this procedure implies introducing a deformation field that has been computed using periodic boundary conditions on a bulklike $1 \times 1 \times 1$ cell into an infinite medium with the same elastic constants but different boundary conditions (nonperiodic). This is therefore a slightly inconsistent procedure that can only be justified *a posteriori* by the agreement between the energies obtained from the *ab initio* calculations and the FE approach (see below).

All the FE simulations have been performed with the program COMSOL MULTIPHYSICS,[31] using 0.15 Å wide triangular elements. Figure 5 gives the diagonal components of the stress tensor for H in O-site and T-site (the origin of distances is located at the surface of the deformed $1 \times 1 \times 1$ region). Both cases show very little residual stress beyond 6 Å (which corresponds to the $3 \times 3 \times 3$ supercell). The elastic energy distribution associated with these stresses is well converged at these distances (Table III); contributions from larger regions only amount to 1 or 2% of the total elastic energy. This result shows why it is not necessary to go beyond the $3 \times 3 \times 3$ supercell in our *ab initio* simulations. The stress distributions are very different for H in O-site and

TABLE III. Elastic energy distribution (meV) and fractional contribution to the total one (%) calculated by finite elements over $n \times n \times n$ regions ($n=2,3,4,5$). Residual energy beyond $n=3$ is below 3% of the total one.

O-site		$2\times$	$3\times$	$4\times$	$5\times$
	E(meV)	195	215	219	221
	%	88	9	2	0.8
T-site		$2\times$	$3\times$	$4\times$	$5\times$
	E(meV)	23	24	24	24
	%	95	4	0.7	0.3

in T-site: The former is very anisotropic ($x \sim y \neq z$) and its maximum value is ≈ 2 times the maximum value for T-site. The stored elastic energy, quadratic on the stress tensor, is approximately ten times higher for H in the O-site (Table III). Therefore, storing one H atom in the O-site costs about 0.2 eV to deform the surrounding cells if compared with absorption in the T-site. This number agrees well with the value previously obtained from the *ab initio* simulation, ≈ 0.1 eV for a fully relaxed lattice, justifying the interpretation derived from these calculations. This approach shows that the main difference between absorption in the T-site and O-site is related to the relaxation of elastic energy in neighboring cells. Only if all the cells are deformed in the same way, i.e., when the system does not need to invest energy again the elastic properties of the surrounding cells, the O-site may become the preferred one.

V. CONCLUSIONS

For the case of high concentrations of interstitial H in bcc iron, a large bct distortion is found favorable with H absorbing preferentially in the octahedral site. This distortion is only possible if the hydrogen concentration is high enough to transform a significant number of unit cells from bcc to bct. This transformation might form a precursor to the bcc to fcc phase transformation. For the case of low concentration of interstitial H, the energetic cost of deforming the surrounding iron matrix makes preferable absorption in the T-site. Hydrogen diffuses faster around regions of high concentration, where the transition state is located between the T-site and O-site. In low-concentration regions, diffusion takes place between the T-site, avoiding the O-site (a local maximum). H absorbed in O-site or T-site create a completely different distribution of stresses in neighboring cells explaining the preference of H for the T-site for cases or regions of low concentration of interstitials.

ACKNOWLEDGMENTS

[1] N. Eliaz, A. Shachar, B. Tal, and D. Eliezer, Eng. Failure Anal. **9**, 167 (2002).

[2] M. Elices, J. Mater. Sci. **39**, 3889 (2004).

[3] Y. Liang, P. Sofronis, and N. Aravas, Acta Mater. **51**, 2717 (2003).

[4] L. Pauling, *The Nature of the Chemical Bond*, 3rd ed. (Cornell University Press, Ithaca, 1986).

[5] C. Barret and T. Massalski, *Structure of Metals: Crystallographic Methods, Principles and Data*, 3rd ed. (Pergamon, Oxford, 1987).

[6] R. Griessen, Phys. Rev. B **38**, 3690 (1988).

[7] J. K. Norskov, Phys. Rev. B **26**, 2875 (1982).

[8] A. L. Companion, F. Liu, and D. P. Onwood, J. Less-Common Met. **107**, 131 (1985).

[9] C. Minot and C. Demangeat, J. Chem. Phys. **86**, 2161 (1987).

[10] C. Elsasser, J. Zhu, S. G. Louie, M. Fahnle, and C. Chan, J. Phys.: Condens. Matter **10**, 5081 (1998).

[11] A. Juan and R. Hoffmann, Surf. Sci. **421**, 1 (1999).

[12] D. E. Jiang and E. A. Carter, Phys. Rev. B **70**, 064102 (2004).

[13] X. gao Gong, Z. Zeng, and Q. qi Zheng, J. Phys.: Condens. Matter **1**, 7577 (1989).

[14] M. J. Puska and R. M. Nieminen, Phys. Rev. B **29**, 5382 (1984).

[15] V. E. Antonov, K. Cornell, V. K. Fedotov, A. I. Kolesnikov, E. G. Ponyatovsky, V. I. Shiryaev, and H. Wipi, J. Alloys Compd. **264**, 214 (1998).

[16] M. Castellote *et al.*, Nucl. Instrum. Methods Phys. Res. B **259**, 975 (2007).

[17] K. Kiuchi and R. B. McLellan, Acta Metall. **31**, 961 (1983).

[18] P. Hohenberg and W. Kohn, Phys. Rev. **136**, B864 (1964).

[19] D. Vanderbilt, Phys. Rev. B **41**, 7892 (1990).

[20] H. J. Monkhorst and J. D. Pack, Phys. Rev. B **13**, 5188 (1976).

[21] S. J. Clark, M. D. Segall, C. J. Pickard, P. J. Hasnip, M. J. Probert, K. Refson, and M. C. Payne, Z. Kristallogr. **220**, 567 (2005).

[22] CASTEP 4.2, http://www.accelrys.com

[23] J. P. Perdew, K. Burke, and M. Ernzerhof, Phys. Rev. Lett. **77**, 3865 (1996).

[24] N. Marzari, D. Vanderbilt, and M. C. Payne, Phys. Rev. Lett. **79**, 1337 (1997).

[25] *Handbook of Chemistry and Physics*, 88th ed. edited by D. R. Lide (CRC, London, 2007).

[26] W. Press, S. Teukolsky, W. Vetterling, and B. Flannery, *Numerical Recipes: The Art of Scientific Computing* (Cambridge Univesity Press, Cambridge, 2007).

[27] B. Pfrommer, M. Cote, S. Louie, and M. Cohen, J. Comput. Phys. **131**, 233 (1997).

[28] M. Blanco-Rey and P. de Andres, Surf. Sci. **600**, L91 (2006).

[29] V. L. Sliwko, P. Mohn, K. Schwarz, and P. Blaha, J. Phys.: Condens. Matter **8**, 799 (1996).

[30] T. Halgren and W. Lipscomb, Chem. Phys. Lett. **49**, 225 (1977).

[31] COMSOL MULTIPHYSICS 3.4, http://www.comsol.com/